ACS SENSORS

Article

Cite This: ACS Sens. 2018, 3, 1531−1538

pubs.acs.org/acssensors

Plant Biomarker Recognition by Molecular Imprinting Based Localized Surface Plasmon Resonance Sensor Array: Performance Improvement by Enhanced Hotspot of Au Nanostructure

Liang Shang,[†] Chuanjun Liu,[†,‡] Bin Chen,[§] and Kenshi Hayashi*[,†]

[†]Department of Electronics, Graduate School of Information Science and Electrical Engineering, Kyushu University, Fukuoka 819-0395, Japan

[‡]Research Laboratory, U.S.E. Co., Ltd., Tokyo 150-0013, Japan

[§]College of Electronic and Information Engineering, Southwest University, Chongqing 400715, China

Supporting Information

ABSTRACT: Detection of plant volatile organic compounds (VOCs) enables monitoring of pests and diseases in agriculture. We previously revealed that a localized surface plasmon resonance (LSPR) sensor coated with a molecularly imprinted sol−gel (MISG) can be used for cis-jasmone vapor detection. Although the selectivity of the LSPR sensor was enhanced by the MISG coating, its sensitivity was decreased. Here, gold nanoparticles (AuNPs) were doped in the MISG to enhance the sensitivity of the LSPR sensor through hot spot generation. The size and amount of AuNPs added to the MISG were investigated and optimized. The sensor coated with the MISG containing 20 μL of 30 nm AuNPs exhibited higher sensitivity than that of the sensors coated with other films. Furthermore, an optical multichannel sensor platform containing different channels that were bare and coated with four types of MISGs was developed to detect plant VOCs in single and binary mixtures. Linear discriminant analysis, k-nearest neighbor (KNN), and naïve Bayes classifier approaches were used to establish plant VOC identification models. The results indicated that the KNN model had good potential to identify plant VOCs quickly and efficiently (96.03%). This study demonstrated that an LSPR sensor array coated with a AuNP-embedded MISG combined with a pattern recognition approach can be used for plant VOC detection and identification. This research is expected to provide useful technologies for agricultural applications.

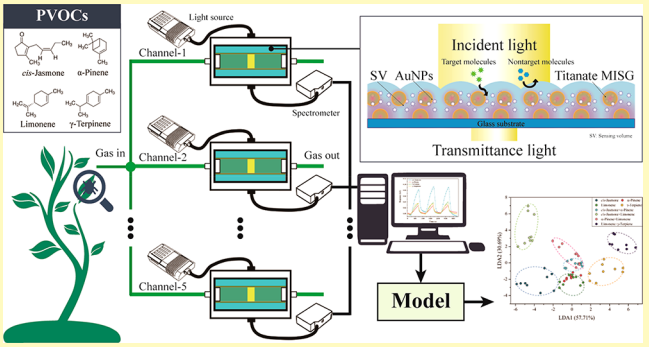

KEYWORDS: *plant volatile organic compounds, localized surface plasma resonance, molecularly imprinted sol−gel, hot spot effect, optical sensor array, pattern recognition*

Plants can release volatile organic compounds (VOCs) as biomarkers from leaves, flowers, roots, and other tissues to the environment through a variety of complicated mechanisms.[1−3] It has been confirmed that plant VOCs play an ecological role in attraction of species-specific pollinators and mediation of tritrophic interactions in terrestrial ecosystems.[4] Furthermore, pest damage and disease can cause changes in plant VOCs that help with self-healing, mechanical wounding, herbivore feeding, infection by pathogens, and repelling pests.[5,6] In 1983, Rhoades and colleagues speculated that willows can release some airborne signals as a type of "plant-to-plant communication" to warn their neighbors of upcoming danger.[7] Their hypothesis was confirmed soon after by Baldwin in a study on poplars.[8] Plant VOCs mainly consist of terpenes such as *cis*-jasmone (CJ), α-pinene, limonene, and γ-terpinene.[9−13] The emission rate of plant VOCs strongly depends on environmental conditions and stressor agents.[14,15] Therefore, detection of plant VOCs in the environment can be used for pest and disease monitoring in agriculture. Plant VOCs are currently detected and analyzed by gas chromatography/mass spectrometry or gas chromatography electroantennographic detection.[16−18] However, these methods are not suitable for real-time plant VOC monitoring because they are costly, time-consuming, and not portable. Consequently, sensors for real-time detection of plant VOCs with high sensitivity, fast response speed, and interference immunity need to be developed for agricultural applications.

Localized surface plasmon resonance (LSPR) is a phenomenon that involves collective electron charge oscillations at noble metal nanoparticle (NP) surfaces, which has been used as a transducer by converting changes in refractive index (RI) into spectral shifts.[19−22] LSPR based on this mechanism shows

Received: April 24, 2018
Accepted: August 3, 2018
Published: August 3, 2018

DOI: 10.1021/acssensors.8b00329
ACS Sens. 2018, 3, 1531−1538

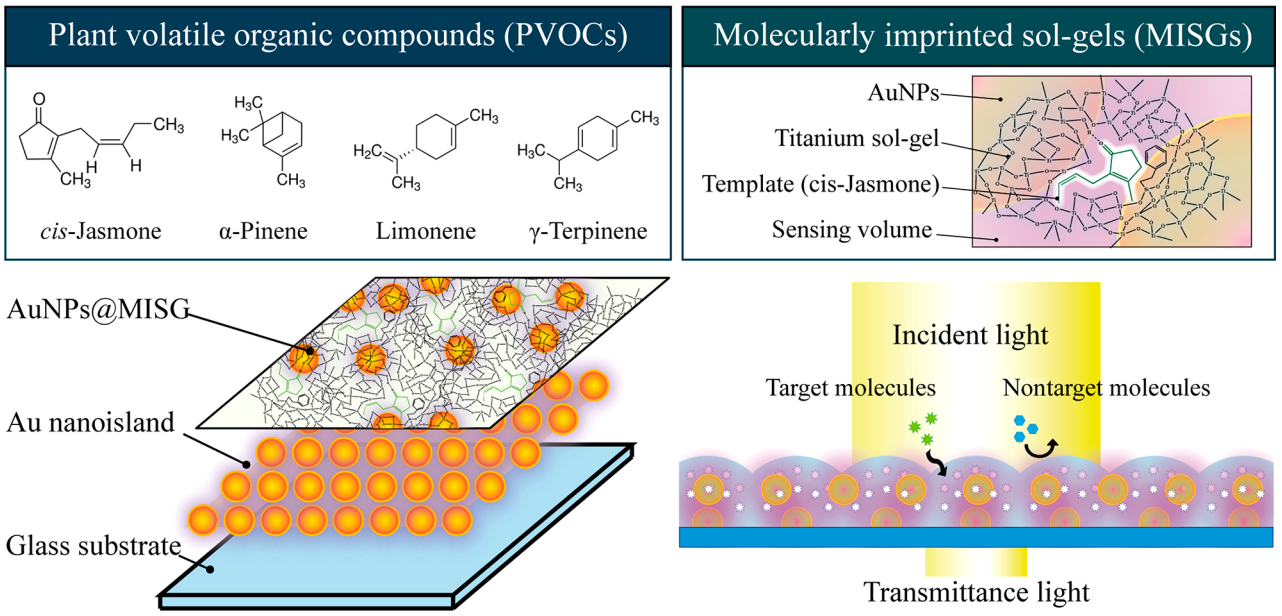

Figure 1. Schematic of AuNPs@MISG-coated Au nanoislands for selective plant VOC detection.

great potential in a wide range of applications, such as drug delivery, biological imaging, metal ion detection, and biosensors, because of its rapid response and high sensitivity.[23−29] However, nonspecificity limited their applications. Therefore, absorption materials, such as molecularly imprinted polymers, are applied for enhancing the selectivity for LSPR sensors. Our former study revealed that a molecularly imprinted sol−gel (MISG)-coated LSPR sensor was effective for CJ vapor detection.[30] In the sol−gel process, based on the interaction (hydrogen bond, $\pi-\pi$ bond, and van der Waals) between the functional groups of template molecules and the functional monomer in titanium oxide sols, templates can be covered by TiO_2 matrix. By removing these template molecules, the cavities similar to the target molecules can be remained in the sol−gel matrix for enhancing the selectivity of sensors. Although the selectivity of the sensor was enhanced by the MISG coating, its sensitivity was decreased. Recently, molecularly imprinted polymers have been combined with gold nanoparticles (AuNPs) to amplify the LSPR causing the hot spot effect.[31] Based on the LSPR coupling between AuNPs in an MIP and a thin gold film, RI changes can be enhanced for use in optical sensing.[32] Therefore, AuNPs embedded in an MISG (denoted as AuNPs@MISG) should be effective at enhancing the signal intensity of a sensor while maintaining high selectivity. In addition, considering the complex nature of the agricultural environment, a multichannel sensor array combined with a pattern recognition method should be developed for plant VOC identification.

The primary goal of this research is to develop a AuNPs@MISG LSPR sensor platform to detect and identify plant VOCs. As illustrated in Figure 1, the sensor consists of an LSPR sensing layer coated with an MISG layer. The LSPR sensing layer is fabricated by vacuum sputtering and annealing. An AuNPs@MISG layer is formed around the AuNPs in the sensing layer by spin coating. Sensor responses are captured by monitoring changes in the RI by absorbance spectra. AuNPs doped in the MISG are expected to increase the signal intensity through the hot spot effect. Critical parameters of the AuNPs@MISG (AuNP size, amount, and spin coating speed) are tuned to optimize sensitivity. By spin coating MISG solutions with diverse template molecules on AuNPs, a multichannel optical sensor platform for plant VOC identification is constructed. The identification capability of the sensor platform is tested using four plant VOCs (CJ, α-pinene, limonene, and γ-terpinene) and their binary mixtures. Principal component analysis (PCA) and linear discriminant analysis (LDA) are used to visualize the cluster trends of vapor samples in low dimensions. To assess the potential of the sensor platform, three common supervised approaches, LDA, k-nearest neighbor (KNN), and naïve Bayes classifier (NBC), are used to establish plant VOC identification models. The objective of this study is to develop a new sensing strategy for plant VOC detection in agricultural applications.

MATERIALS AND METHODS

Materials, Chemicals, and Instrumentation. Titanium tetrabutoxide (TBOT), isopropanol, CJ, limonene, γ-terpinene, titanium tetrachloride ($TiCl_4$), acetone, and ethanol were purchased from Wako Pure Chemical Industries Co., Ltd. (Osaka, Japan). (3-Aminopropyl)triethoxysilane (APTES) was purchased from Shin-Etsu Chemical Co., Ltd. (Tokyo, Japan). AuNP suspensions (NP diameter: 10, 20, 30, and 40 nm, stabilized suspension in citrate buffer, concentrations: 6.0×10^{12}, 6.54×10^{11}, 1.8×10^{11}, and 7.2×10^{10} particles/mL), α-pinene, and trimethoxyphenylsilane (TMPS) were purchased from Sigma-Aldrich (St. Louis, MO). All reagents were used as received. Scanning electron microscopy (SEM; SU8000, Hitachi, Japan) was used to image sensor morphology.

Preparation of AuNPs@MISG Reaction Solution. The MISG reaction solutions were prepared as reported previously.[30] First, TBOT (0.441 mmol, 150 μL) was dissolved in isopropanol (2 mL) as a precursor. Then, CJ, α-pinene, limonene, or γ-terpinene (50 μL) as a template material and TMPS (0.252 mmol, 50 μL) as a functional monomer were added with stirring. $TiCl_4$ (0.132 mmol, 25 μL) was added to initiate the reaction and then the MISG reaction solution was prehydrolyzed in a water bath at 60 °C for 1 h with stirring. The mixture was vigorously stirred for 8 h at room temperature (20 °C) to complete the MISG reaction. Finally, AuNP suspension (50 μL) was added to the hydrolyzed MISG solution while stirring. Before spin coating, the reaction solution was stirred at room temperature for 8 h.

AuNPs@MISG-Coated LSPR Sensor Fabrication. The LSPR substrates were prepared as reported previously.[33] Briefly, a glass

DOI: 10.1021/acssensors.8b00329
ACS Sens. 2018, 3, 1531−1538

substrate (12 × 9 mm) was ultrasonically cleaned in ultrapure water, acetone, and ethanol and then immersed in a 1:10 (v:v) APTES/ethanol solution for 8 h. After being cleaned with ethanol and dried with flowing nitrogen, a 3 nm thick layer of AuNPs was deposited using a quick coater (SC-701 HMCII, Sanyu Electron, Japan). The substrate was heated in a muffle furnace (SSTS-13K, ISUZU, Seisakusho, Japan) at 500 °C for 2 h and then cooled to room temperature. The sample was sputtered and annealed again under the same conditions to form a high-sensitivity LSPR substrate.[34] The MISG reaction solution (20 μL) was then spin-coated on the AuNP layer for 1 min. Finally, the sample was annealed at 130 °C for 1 h to complete MISG fabrication and evaporate the template molecules. All samples were stored under vacuum to remove VOCs from the MISG.

Sensing System and Software. The vapor generation and sensing systems used in this study were similar to those in our previous study.[33] Plant VOC vapor was generated from a glass bottle with odorants (2 mL) using the headspace method and then controlled by two mass flow controllers with a LabView system (2014, National Instruments, Austin, USA). The concentrations C of plant VOCs (in ppm) were calculated by

$$C = \frac{k \times D_r \times 10^3}{F} \quad (1)$$

where D_r is the diffusion rate (μg/min), F is the flow rate of the diluent air (L/min), and k is the factor used to convert gas weight to gas volume, which is defined by

$$k = \frac{22.4 \times (273 + t) \times 760}{M \times 273 \times P} \quad (2)$$

Here, M is the molecular weight of the plant VOC molecule, t is the temperature of the gas chamber (°C), and P is the gas pressure (760 mmHg). A customized optical sensing system was used in the present study. Absorption spectra were acquired over the range of 400−900 nm at a resolution of 0.1 nm and recorded by OPwave+ software (Ocean Optics). The plant VOC vapor flow was switched on for 600 s and then switched to clean air for 600 s during all the test cycles. The response matrix from the AuNPs@MISG LSPR sensor array was processed and analyzed by R (version 3.4.3). The KNN, LDA, and NBC models were established using R packages (e1071, MASS, and caret).

RESULTS AND DISCUSSION

Effect of Au NP Size on LSPR. Because the size of AuNPs is a critical factor affecting their LSPR signals, MISG-coated AuNPs with diameters of 10, 20, 30, and 40 nm were considered. The typical features of the MISG-coated samples were analyzed using UV−vis spectroscopy and SEM, as shown in Figures S1 and S2, respectively. Relative to that of the MISG-coated sample, the LSPR peaks of the AuNPs@MISG-coated samples were blue-shifted. In addition, the surfaces of the AuNPs@MISG-coated samples varied with the AuNP size, indicating that the sol−gel process was affected by the diameter of the AuNPs. The responses of the MISG- and AuNPs@MISG-coated samples to CJ vapor were measured by the change of absorption ΔA, which was calculated using

$$\Delta A = A_{gas} - A_{air} \quad (3)$$

where A_{air} is the absorption in air and A_{gas} is the absorption in the plant VOC vapor. The sensitivity to CJ vapor of various MISG-coated samples is summarized in Figure 2. The MISG without AuNPs offered lower sensitivity than that of the AuNPs@MISG-coated samples, revealing that the AuNPs improved the response of the MISG to target molecules. The response of AuNPs@MISG-coated sensor with 30 nm AuNPs was 6.33 times that of the one without NPs. An SEM image of a AuNP layer is illustrated in Figure S3a. The particle size

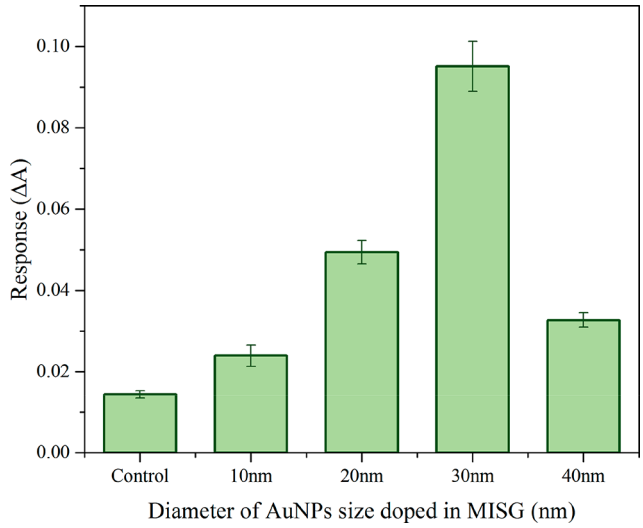

Figure 2. Response affected by Au nanoparticle size in MISGs.

distribution histogram of the spherical AuNPs was analyzed by ImageJ (Figure S4). The analysis indicated that the diameter of the AuNPs on the substrate was 34.13 ± 9.41 nm, which is close to that of the AuNPs in the MISG (30 nm). The high sensitivity of the sensor was therefore caused by hot-spot coupling between the AuNPs on the substrate surface and those in the MISG. Therefore, 30 nm is the optimal size for the AuNPs in the MISG.

Optimization of the Amount of AuNPs. To obtain the best performance for plant VOC detection, the effect of the amount of AuNPs on sensing behavior was investigated. UV−vis spectra and SEM images of MISG samples with different amounts of AuNPs are presented in Figure S5 and S6, respectively. The responses of the AuNPs@MISG-coated samples to CJ vapor were measured and are depicted in Figure 3. Evidently, the sensitivity of the sensors increased with the AuNP concentration initially and then decreased. The results revealed that the sensor coated with the MISG containing 20 μL of 30 nm AuNPs had the highest sensitivity of those investigated.

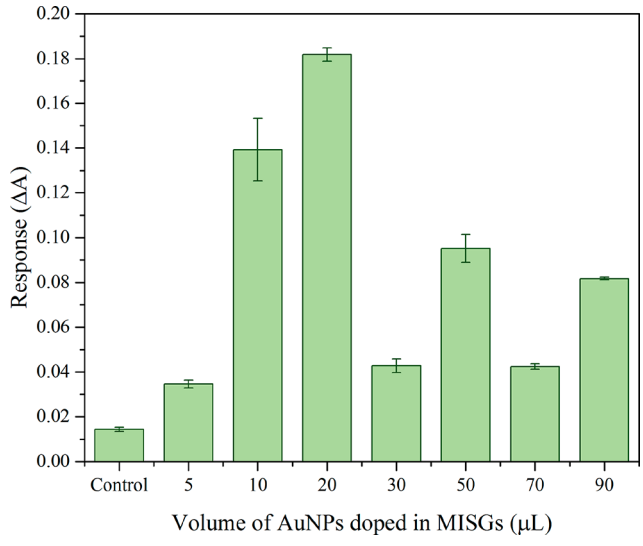

Figure 3. Response affected by Au nanoparticle amount in MISGs.

DOI: 10.1021/acssensors.8b00329
ACS Sens. 2018, 3, 1531−1538

Optimization of Spin Coating Speed. The thickness of the sensing film influences the sensitivity of LSPR sensors.[35] Here, spin coating speeds of 2000, 3000, 4000, and 5000 rpm were selected to optimize the thickness of the AuNPs@MISG coatings. The sensitivities to CJ vapor of samples coated with the optimal AuNPs@MISG solution at different coating speeds are illustrated in Figure 4. A thinner MISG layer exhibited

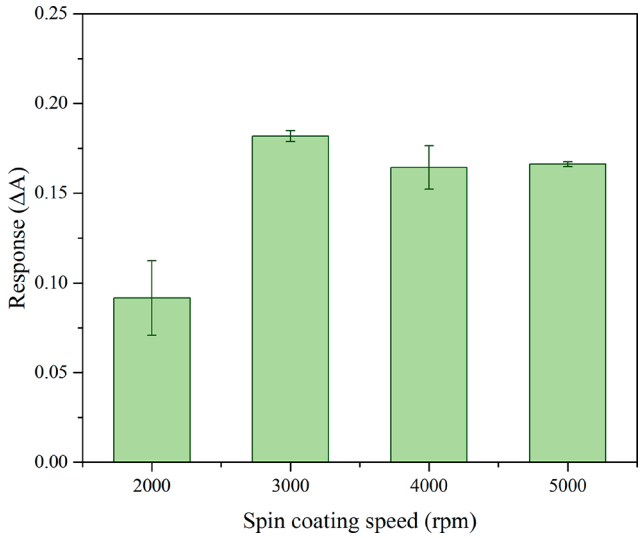

Figure 4. Response affected by spin coating speed.

lower selectivity for target molecules. However, a layer that was too thick would have a long recovery time.[33] Considering the observed sensor responses, the optimal spin coating speed was selected as 3000 rpm in the present study.

CJ Detection with the Optimized AuNPs@MISG-Coated LSPR Sensor. To evaluate the interference immunity of the AuNPs@MISG-coated sensor, it was exposed to the three primary plant VOCs: α-pinene, limonene, and γ-terpinene. All the responses were normalized to the plant VOC concentrations using eq 4:

$$R_{\text{normalized}} = \frac{R}{\lg(C_{\text{test}})} \tag{4}$$

where R is the original sensor response and C_{test} is the concentration of each plant VOC. For CJ, α-pinene, limonene, and γ-terpinene, calculated C_{test} values were 10 ± 1, 188 ± 34, 971 ± 59, and 750 ± 36 ppm, respectively.

The normalized in situ response of the optimized AuNPs @ MISG-coated LSPR sensor to these interferents is shown in Figure 5. The response to CJ was much higher than that to the interfering plant VOCs. This indicates that the developed sensor has sufficient interference immunity for use in agricultural applications.

AuNPs@MISG-Coated LSPR Sensor Array. Although the sensitivity of the sensor was enhanced because of the hot spot effect, the response intensity of the sensor was affected by the high concentrations of interfering plant VOCs. To address this problem, a AuNPs@MISG LSPR sensor array was constructed for identification and detection of plant VOCs. Four types of AuNPs@MISG reaction solutions were prepared using the optimal preparation conditions. By spin coating these solutions at 3000 rpm on the AuNP-coated surface, a sensor array was developed for pattern recognition of plant VOCs (Figure S3). The sensor array included five channels: bare, MISG_{CJ},

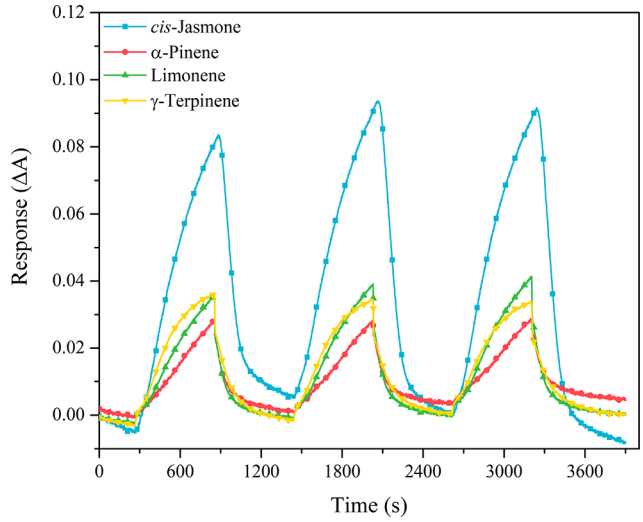

Figure 5. Real-time responses of AuNPs@MISG_{CJ}-modified Au-islands to four types of plant VOCs.

$\text{MISG}_{\alpha\text{-pinene}}$, $\text{MISG}_{\text{limonene}}$, and $\text{MISG}_{\gamma\text{-terpinene}}$. The response characteristics of the array to four single plant VOCs (CJ, α-pinene, limonene, and γ-terpinene) and four binary mixtures (CJ + α-pinene, CJ + limonene, α-pinene + limonene, and limonene + γ-terpinene) were investigated. For each type of vapor, three vapor flow rates (0.3, 0.5, and 0.7 L/min) were measured at each concentration, and the measurements were repeated three times. Therefore, a data set containing 72 samples (8 plant VOCs × 3 flow rates × 3 repeats) was collected for subsequent research. Both plant VOC vapor generation and sensing measurements were performed at room temperature.

Correlation analysis was carried out initially to evaluate the relationship of each channel. The Pearson correlation coefficient was calculated using eq 5,[36]

$$\text{Cor}(\mathbf{x}, \mathbf{y}) = \frac{\sum_{i=1}^{N}(\mathbf{x}_i - \bar{\mathbf{x}})(\mathbf{y}_i - \bar{\mathbf{y}})}{\sqrt{\sum_{i=1}^{N}(\mathbf{x}_i - \bar{\mathbf{x}})^2 \sum_{i=1}^{N}(\mathbf{y}_i - \bar{\mathbf{y}})^2}} \tag{5}$$

where $\mathbf{x}$ and $\mathbf{y}$ indicate the response vectors for two channels; $\bar{\mathbf{X}}$ and $\bar{\mathbf{y}}$ are the mean values of vector $\mathbf{x}$ and $\mathbf{y}$, respectively; and N is the dimension of vector $\mathbf{x}$ or $\mathbf{y}$ (72). Figure 6 reveals there was a low correlation (under 0.4) between the bare and MISG-coated channels, indicating that the bare channel has different information to others. Because the bare LSPR sensor has low selectivity for the target molecules, the response of the bare channel would be related to the concentration of the plant VOCs. In contrast, the responses of the MISG-coated channels contained contributions from the MIP and matrix effects, which increase selectivity for target molecules.

To visualize the clustering trends of vapor samples in low dimensions, PCA was performed on the normalized response matrix ($M_{72\times5}$). The first three principal components (PCs), which captured 84.33% of the cumulative variance proportion of the response data, are plotted in Figure 7. In PCA space, only limonene (PC1−PC2 space, Figure 7a) and γ-terpinene (PC2−PC3 space, Figure 7c) samples formed differentiable clusters. It was difficult to distinguish clearly between the groups for other categories, such as the binary mixtures.

The response matrix was also analyzed by LDA. Unlike PCA, LDA is a supervised approach that aims to achieve an

DOI: 10.1021/acssensors.8b00329
ACS Sens. 2018, 3, 1531−1538

	CH1	CH2	CH3	CH4	CH5
CH1	1	0.06	-0.05	-0.17	-0.34
CH2	0.06	1	0.53	0.31	0.06
CH3	-0.05	0.53	1	0.59	0.1
CH4	-0.17	0.31	0.59	1	0.51
CH5	-0.34	0.06	0.1	0.51	1

Figure 6. Correlation matrix for sensor array. CH1, CH2, CH3, CH4, and CH5 are bare, $MISG_{CJ}$-, $MISG_{\alpha\text{-Pinene}}$-, $MISG_{Limonene}$-, and $MISG_{\gamma\text{-Terpinene}}$-coated samples, respectively.

optimal transformation by minimizing the intragroup distances and maximizing the intergroup distances simultaneously.[37] Figure 8 shows 72 samples from eight clusters plotted in LDA spaces. In the LDA1−LDA2 space (Figure 8a), CJ, γ-terpinene, CJ + limonene, and limonene + γ-terpinene can be separated easily. Considering LDA1−LDA2 and LDA2−LDA3 (Figure 8b) simultaneously, α-pinene and limonene occupied separate regions. We also found overlap between CJ + α-pinene and α-pinene + limonene in all LDA spaces. This means that it is hard to separate the plant VOCs in low-dimension spaces. Therefore, pattern recognition approaches need to be explored and evaluated.

Identification Model Calibration. To investigate the ability of the AuNPs@MISG-coated LSPR sensor array to discriminate various types of plant VOCs, three commonly used classification frameworks (LDA, KNN, and NBC) were used. KNN has been widely applied as a supervised pattern recognition approach because of its robust nature and suitability for limited sample sets.[38] The main assumption of KNN is that the closer the samples, the more likely it is that they belong in the same category.[39,40] Considering the sample size, three nearest neighbors were considered in the present study. Similarly, NBC is a supervised statistical model established by calculating the probability that a given sample belongs to a certain class.[41] Because of its simple structure and ease of implementation, NBC has been widely used.[42] More details on KNN and NBC can be found elsewhere.[43−46]

In this study, 72 samples were divided into calibration and validation sets by the random selection method.[47] Samples from the calibration set were used as training models, and samples from the validation set were used to evaluate the established models. The ratio of samples in the calibration and validation sets was 7:3. Because the sample partition was random, the performance of the model was unstable. Therefore, sample partition was repeated 100 times to overcome this problem. The identification performance of a classification framework was evaluated by accuracy[48] using eq 6,

$$\text{accuracy} = \frac{\text{TPs} + \text{TNs}}{\text{TPs} + \text{TNs} + \text{FPs} + \text{FNs}} \times 100\% \quad (6)$$

where a true positive (TP) is when a positive sample is classified as a positive example, a true negative (TN) is when a negative sample is classified as a negative example, a false positive (FP) is when a negative sample is classified as a positive example, and a false negative (FN) is a positive sample is classified as a negative example. According to the average accuracies, the optimal model was chosen.

The plant VOC identification accuracies for the calibration and validation sets of the three models are listed in Table 1. Other standard performance measures (sensitivity, specificity, precision, recall, and F1 score) are summarized in Tables S1 and S2. For each plant VOC, the LDA model showed the highest average accuracy in identifying CJ (99.40 ± 3.20%), γ-terpinene (99.56 ± 1.02%), and α-pinene + limonene (97.49 ± 3.40%). The KNN model readily identified α-pinene (89.83 ± 8.87%) and limonene (95.57 ± 4.49%). The NBC model exhibited the highest identification accuracy for mixtures, including CJ + α-pinene (95.30 ± 6.34%), CJ + limonene (100%), and limonene + γ-terpinene (100%). This indicates that the NBC model was more suitable to deal with complicated samples than the other models. For the calibration set, the accuracy of the NBC model reached 97.02 ± 2.79%, which was higher than that of the LDA model (86.66 ± 2.49%) and KNN model (95.58 ± 8.06%). For the validation set, KNN had the highest accuracy (97.02 ± 2.79%), followed by LDA (94.72 ± 8.52%) and NBC (94.39 ± 9.15%), indicating that the generalization ability of the KNN model is higher than that of the others. Considering total average accuracy, KNN

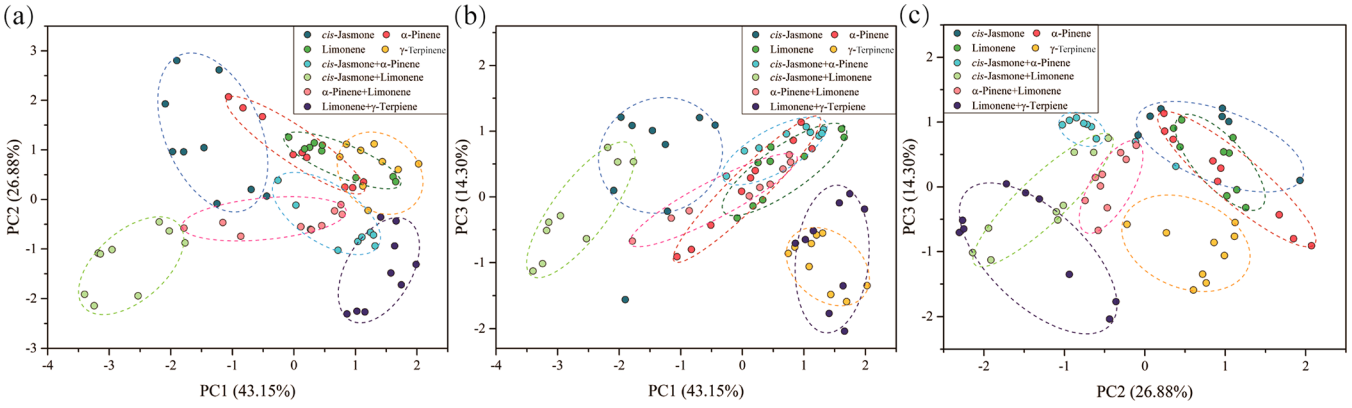

Figure 7. PCA score plots of the responses of 72 samples from four plant VOCs (CJ, α-pinene, limonene, and γ-terpinene) and their binary mixtures (CJ + α-pinene, CJ + limonene, α-pinene + limonene, and limonene + γ-terpinene).

DOI: 10.1021/acssensors.8b00329
ACS Sens. 2018, 3, 1531−1538

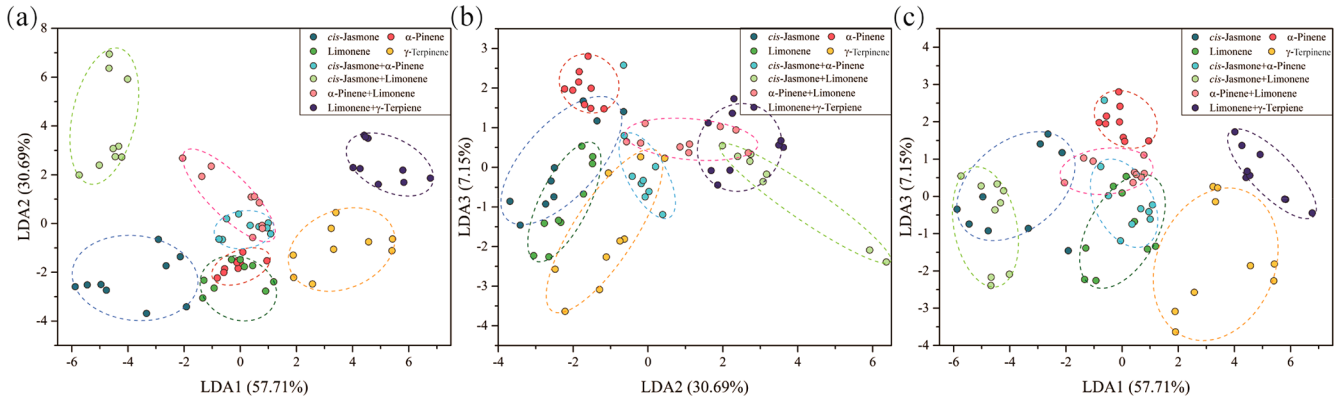

Figure 8. LDA score plot of the first three discriminant factors achieved from the response matrix of 72 samples from four plant VOCs (CJ, α-pinene, limonene, and γ-terpinene) and their binary mixtures (CJ + α-pinene, CJ + limonene, α-pinene + limonene, and limonene + γ-terpinene).

Table 1. Plant VOCs Identification Accuracies of Models Based on the Response Matrix (%)

		calibration set		validation set		total avg	
plant VOCs	modeling approach	mean	SD	mean	SD	mean	SD
CJ	LDA	99.93	0.63	98.87	4.48	99.40	3.20
	KNN	97.54	6.63	96.98	3.53	97.26	5.31
	NBC	96.98	3.53	91.79	11.30	94.39	8.37
α-pinene	LDA	89.98	4.20	86.85	13.13	88.42	9.75
	KNN	91.10	11.69	88.55	4.55	89.83	8.87
	NBC	88.55	4.55	82.74	15.86	85.65	11.67
limonene	LDA	98.78	1.40	93.55	12.81	96.17	9.11
	KNN	97.31	6.29	99.83	0.90	98.57	4.49
	NBC	99.83	0.90	94.54	9.60	97.19	6.82
γ-terpiene	LDA	99.87	0.34	99.24	1.40	99.56	1.02
	KNN	97.60	6.13	99.94	0.63	98.77	4.36
	NBC	99.94	0.63	98.21	4.58	99.08	3.27
CJ + α-pinene	LDA	88.13	4.32	86.86	11.59	87.50	8.75
	KNN	92.98	11.17	96.48	4.29	94.73	8.46
	NBC	96.48	4.29	94.11	7.87	95.30	6.34
CJ + limonene	LDA	99.55	1.60	97.74	5.65	98.65	4.15
	KNN	98.94	3.79	100.0	0.00	99.47	2.68
	NBC	100.0	0.00	100.0	0.00	100.0	0.00
α-pinene + limonene	LDA	97.62	2.20	97.35	4.28	97.49	3.40
	KNN	89.91	10.69	94.40	3.11	92.16	7.87
	NBC	94.40	3.11	93.71	10.77	94.06	7.93
Limonene + γ-terpiene	LDA	99.38	1.88	97.33	6.14	98.36	4.54
	KNN	99.27	2.99	100.0	0.00	99.64	2.11
	NBC	100.0	0.00	100.0	0.00	100.0	0.00
summary	LDA	96.66	2.49	94.72	8.52	95.69	6.28
	KNN	95.58	8.06	97.02	2.79	96.30	6.03
	NBC	97.02	2.79	94.39	9.15	95.71	6.77

had the highest accuracy (96.30 ± 6.03%), followed by LDA (95.69 ± 6.28%) and then NBC (95.71 ± 6.77%). Overall, we found that KNN was the optimal model to identify plant VOCs based on accuracies for the calibration and validation sets. We also found that the lowest accuracy achieved by the models was higher than 95%. This indicated that enough molecular information was captured by the AuNPs@MISG LSPR sensor array to allow plant VOC identification.

Although the developed sensing platform is able to identify plant VOCs, the information captured by the sensor array is still not sufficient to deal with the complicated agricultural environment. We believe that by including more channels in the sensor array with coated with different MIPs and MISGs, an array that is able to handle complicated vapor mixtures could be obtained in the future. In addition, heterostructured AuNPs could be used to further improve sensitivity through the hot spot effect.

CONCLUSIONS

An LSPR sensor coated with an MISG containing AuNPs to amplify the sensing signal was developed for plant VOC detection. The optimal size and amount of AuNPs doped in the MISG were 30 nm and 20 μL, respectively. Under optimal conditions, the sensitivity of the AuNPs@MISG-coated sensor was 12.33 times higher than that of the equivalent without AuNPs, which was caused by hot spot enhancement. The real-time responses of the sensor displayed good interference immunity and repeatability. A five-channel AuNPs@MISG

DOI: 10.1021/acssensors.8b00329
ACS Sens. 2018, 3, 1531−1538

LSPR sensor array was designed to detect and identify four plant VOCs alone and in binary mixtures. Correlation analysis, PCA, and LDA were used to process the response matrix. The results indicated that it was difficult to distinguish clearly between the groups for the binary mixtures. Three supervised modeling approaches (LDA, KNN, and NBC) were used to establish plant VOC pattern recognition models. KNN displayed high accuracy (96.03%), identifying plant VOCs quickly and efficiently. This study demonstrated that a AuNPs@MISG-coated LSPR sensor array combined with a pattern recognition approach can be used for plant VOC detection and identification, which may become a useful technology for agricultural applications.

■ ASSOCIATED CONTENT

Supporting Information

The Supporting Information is available free of charge on the ACS Publications website at DOI: 10.1021/acssensors.8b00329.

Absorption spectra; SEM images; particle size distribution histogram; standard performace measures of LDA, KNN, and NBC models (PDF)

■ AUTHOR INFORMATION

Corresponding Author

*E-mail: hayashi@ed.kyushu-u.ac.jp.

ORCID

Liang Shang: 0000-0001-8369-3049

Kenshi Hayashi: 0000-0001-8679-4953

Notes

The authors declare no competing financial interest.

■ ACKNOWLEDGMENTS

This research was supported by a grant from the China Scholarship Council (CSC), Japan Society for the Promotion of Science (JSPS) KAKENHI (Grant Number 15H01713 and 15H01695), and Chongqing Postdoctoral Science Foundation (Grant Number Xm2017101).

■ REFERENCES

(1) Mothershead, K.; Marquis, R. J. Fitness Impacts of Herbivory Through Indirect Effects on Plant-pollinator Interactions in Oenothera Macrocarpa. *Ecology* **2000**, *81*, 30−40.

(2) Sobhy, I. S.; Woodcock, C. M.; Powers, S. J.; Caulfield, J. C.; Pickett, J. A.; Birkett, M. A. Cis-Jasmone Elicits Aphid-induced Stress Signalling in Potatoes. *J. Chem. Ecol.* **2017**, *43*, 39−52.

(3) Shimotori, Y.; Hoshi, M.; Okabe, H.; Miyakoshi, T.; Kanamoto, T.; Nakashima, H. Synthesis, Odour Characteristics and Antibacterial Activities of the Stereoisomeric Forms of Whisky Lactone and Its Thiono Analogues. *Flavour Fragrance J.* **2017**, *32*, 29−35.

(4) Calfapietra, C.; Fares, S.; Loreto, F. Volatile Organic Compounds from Italian Vegetation and Their Interaction with Ozone. *Environ. Pollut.* **2009**, *157*, 1478−1486.

(5) Holopainen, J. K.; Gershenzon, J. Multiple Stress Factors and the Emission of Plant VOCs. *Trends Plant Sci.* **2010**, *15*, 176−184.

(6) Hoebeke, E. R.; Smith, D. R.; Goulet, H. Athalia Cornubiae Benson (Hymenoptera: Tenthredinidae: Allantinae), a Sawfly Genus and Species New to North America. *Proc. Entomol. Soc. Wash.* **2011**, *113*, 309−314.

(7) Rhoades, D. F. Herbivore Population Dynamics and Plant Chemistry [Phytophagous insects]. In *Variable Plants and Herbivores in Natural and Managed Systems*; Elsevier: 1983; p 155, .

(8) Baldwin, I. T.; Preston, C. A. The Eco-physiological Complexity of Plant Responses to Insect Herbivores. *Planta* **1999**, *208*, 137−145.

(9) Bruinsma, M.; Posthumus, M. A.; Mumm, R.; Mueller, M. J.; van Loon, J. J. A.; Dicke, M. Jasmonic Acid-induced Volatiles of Brassica Oleracea Attract Parasitoids: Effects of Time and Dose, and Comparison with Induction by Herbivores. *J. Exp. Bot.* **2009**, *60*, 2575−2587.

(10) Garbuzov, M.; Ratnieks, F. L. W. Quantifying Variation Among Garden Plants in Attractiveness to Bees and Other Flower-visiting Insects. *Funct. Ecol.* **2014**, *28*, 364−374.

(11) Pickett, J. A.; Khan, Z. R. Plant Volatile-mediated Signalling and Its Application in Agriculture: Successes and Challenges. *New Phytol.* **2016**, *212*, 856−870.

(12) Han, Z. X.; Rana, M. M.; Liu, G. F.; Gao, M. J.; Li, D. X.; Wu, F. G.; Li, X. B.; Wan, X. C.; Wei, S. Green Tea Flavour Determinants and Their Changes Over Manufacturing Processes. *Food Chem.* **2016**, *212*, 739−748.

(13) da Graca, J. P.; Ueda, T. E.; Janegitz, T.; Vieira, S. S.; Salvador, M. C.; de Oliveira, M. C. N.; Zingaretti, S. M.; Powers, S. J.; Pickett, J. A.; Birkett, M. A.; Hoffmann-Campo, C. B. The Natural Plant Stress Elicitor Cis-jasmone Causes Cultivar-dependent Reduction in Growth of the Stink Bug, Euschistus Heros and Associated Changes in Flavonoid Concentrations in Soybean, Glycine Max. *Phytochemistry* **2016**, *131*, 84−91.

(14) Graham, K. K.; Brown, S.; Clarke, S.; Rose, U. S. R.; Starks, P. T. The European Wool-carder Bee (Anthidium Manicatum) Eavesdrops on Plant Volatile Organic Compounds (VOCs) During Trichome Collection. Behav. *Behav. Processes* **2017**, *144*, 5−12.

(15) Bison, J. V.; Cardoso-Gustavson, P.; de Moraes, R. M.; da Silva Pedrosa, G.; Cruz, L. S.; Freschi, L.; de Souza, S. R. Volatile Organic Compounds and Nitric Oxide as Responses of a Brazilian Tropical Species to Ozone: the Emission Profile of Young and Mature Leaves. *Environ. Sci. Pollut. Res.* **2018**, *25*, 3840−3848.

(16) Mesquita, P. R. R.; Nunes, E. C.; dos Santos, F. N.; Bastos, L. P.; Costa, M.; de M. Rodrigues, F.; de Andrade, J. B. Discrimination of Eugenia Uniflora L. Biotypes Based on Volatile Compounds in Leaves Using HS-SPME/GC-MS and Chemometric Analysis. *Microchem. J.* **2017**, *130*, 79−87.

(17) Wiebelhaus, N.; Hamblin, D.; Kreitals, N. M.; Almirall, J. R. Differentiation of Marijuana Headspace Volatiles From Other Plants and Hemp Products Using Capillary Microextraction of Volatiles (CMV) Coupled to Gas-chromatography-mass spectrometry (GC-MS). *Forensic Chem.* **2016**, *2*, 1−8.

(18) Cheung, W. H. K.; Pasamontes, A.; Peirano, D. J.; Zhao, W. X.; Grafton-Cardwell, E. E.; Kapaun, T.; Yokomi, R. K.; Simmons, J.; Doll, M.; Fiehn, O.; Dandekar, A. M.; Davis, C. E. Volatile Organic Compound (VOC) Profiling of Citrus Tristeza Virus Infection in Sweet Orange Citrus Varietals Using Thermal Desorption Gas Chromatography Time of Flight Mass Spectrometry (TD-GC/TOF-MS). *Metabolomics* **2015**, *11*, 1514−1525.

(19) Alula, M. T.; Karamchand, L.; Hendricks, N. R.; Blackburn, J. M. Citrate-capped Silver Nanoparticles as a Probe for Sensitive and Selective Colorimetric and Spectrophotometric Sensing of Creatinine in Human Urine. *Anal. Chim. Acta* **2018**, *1007*, 40−49.

(20) Lin, T. R.; Zhang, M. Q.; Xu, F. H.; Wang, X. Y.; Xu, Z. F.; Guo, L. Q. Colorimetric Detection of Benzoyl Peroxide Based on the Etching of Silver Nanoshells of Au@Ag Nanorods. *Sens. Actuators, B* **2018**, *261*, 379−384.

(21) Guo, L. M.; Li, Z.; Marcus, K.; Navarro, S.; Liang, K.; Zhou, L.; Mani, P. D.; Florczyk, S. J.; Coffey, K. R.; Orlovskaya, N.; Sohn, Y. H.; Yang, Y. Periodically Patterned Au-TiO2 Heterostructures for Photoelectrochemical Sensor. *ACS Sens.* **2017**, *2*, 621−625.

(22) Masson, J. F. Surface Plasmon Resonance Clinical Biosensors for Medical Diagnostics. *ACS Sens.* **2017**, *2*, 16−30.

(23) Kim, G. W.; Ha, J. W. Effect of Adsorbate Electrophilicity and Spiky Uneven Surfaces on Single Gold Nanourchin-based Localized Surface Plasmon Resonance Sensors. *Chem. Phys. Lett.* **2018**, *697*, 38−42.

DOI: 10.1021/acssensors.8b00329
ACS Sens. 2018, 3, 1531−1538

(24) Kim, H. M.; Nam, K. T.; Lee, S. K.; Park, J. H. Fabrication and Measurement of Microtip-array-based LSPR Sensor Using Bundle Fiber. Sens. *Sens. Actuators, A* **2018**, *271*, 146−152.
(25) Lee, B.; Park, J. H.; Byun, J. Y.; Kim, J. H.; Kim, M. G. An Optical Fiber-based LSPR Aptasensor for Simple and Rapid In-situ Detection of Ochratoxin A. *Biosens. Bioelectron.* **2018**, *102*, 504−509.
(26) Shrivas, K.; Nirmalkar, N.; Thakur, S. S.; Deb, M. K.; Shinde, S. S.; Shankar, R. Sucrose Capped Gold Nanoparticles As a Plasmonic Chemical Sensor Based on Non-Covalent Interactions: Application for Selective Detection of Vitamins B-1 And B-6 in Brown and White Rice Food Samples. *Food Chem.* **2018**, *250*, 14−21.
(27) Ding, Z. T.; Stubbs, J. M.; McRae, D.; Blacquiere, J. M.; Lagugne-Labarthet, F.; Mittler, S. A Mass-Producible and Versatile Sensing System: Localized Surface Plasmon Resonance Excited by Individual Waveguide Modes. *ACS Sens.* **2018**, *3*, 334−341.
(28) Yan, Y.; Meng, L. Y.; Zhang, W. Q.; Zheng, Y.; Wang, S.; Ren, B.; Yang, Z. L.; Yan, X. M. High-Throughput Single-Particle Analysis of Metal-Enhanced Fluorescence in Free Solution Using Ag@SiO2 Core-Shell Nanoparticles. *ACS Sens.* **2017**, *2*, 1369−1376.
(29) Zhang, L.; Wang, J. H.; Zhang, J. X.; Liu, Y. Q.; Wu, L. Z.; Shen, J. J.; Zhang, Y.; Hu, Y. L.; Fan, Q. L.; Huang, W.; Wang, L. H. Individual Au-nanocube Based Plasmonic Nanoprobe for Cancer Relevant MicroRNA Biomarker Detection. *ACS Sens.* **2017**, *2*, 1435−1440.
(30) Shang, L.; Liu, C.; Chen, B.; Hayashi, K. Development of Molecular Imprinted Sol-gel Based LSPR Sensor for Detection of Volatile Cis-Jasmone in Plant. *Sens. Actuators, B* **2018**, *260*, 617−626.
(31) Ahmad, R.; Griffete, N.; Lamouri, A.; Felidj, N.; Chehimi, M. M.; Mangeney, C. Nanocomposites of Gold Nanoparticles@ molecularly Imprinted Polymers: Chemistry, Processing, and Applications in Sensors. *Chem. Mater.* **2015**, *27*, 5464−5478.
(32) Qiu, J. J.; Wei, W. D. Surface Plasmon-mediated Photothermal Chemistry. *J. Phys. Chem. C* **2014**, *118*, 20735−20749.
(33) Shang, L.; Liu, C. J.; Watanabe, M.; Chen, B.; Hayashi, K. LSPR Sensor Array Based on Molecularly Imprinted Sol-gels for Pattern Recognition of Volatile Organic Acids. Sens. *Sens. Actuators, B* **2017**, *249*, 14−21.
(34) Chen, B.; Mokume, M.; Liu, C. J.; Hayashi, K. Structure and Localized Surface Plasmon Tuning of Sputtered Au Nano-islands Through Thermal Annealing. *Vacuum* **2014**, *110*, 94−101.
(35) Chen, B.; Liu, C. J.; Hayashi, K. Selective Terpene Vapor Detection Using Molecularly Imprinted Polymer Coated Au Nanoparticle LSPR Sensor. *IEEE Sens. J.* **2014**, *14*, 3458−3464.
(36) Shang, L.; Liu, C.; Tomiura, Y.; Hayashi, K. Odorant Clustering Based on Molecular Parameter-feature Extraction and Imaging Analysis of Olfactory Bulb Odor Maps. Sens. *Sens. Actuators, B* **2018**, *255*, 508−518.
(37) Mungkarndee, R.; Techakriengkrai, I.; Tumcharern, G.; Sukwattanasinitt, M. Fluorescence Sensor Array for Identification of Commercial Milk Samples According to Their Thermal Treatments. *Food Chem.* **2016**, *197*, 198−204.
(38) Acharya, U. R.; Bhat, S.; Koh, J. E. W.; Bhandary, S. V.; Adeli, H. A Novel Algorithm to Detect Glaucoma Risk Using Texton and Local Configuration Pattern Features Extracted From Fundus Images. *Comput. Biol. Med.* **2017**, *88*, 72−83.
(39) Pashchenko, I. N.; Sokolovsky, K. V.; Gavras, P. Machine Learning Search for Variable Stars. *Mon. Not. R. Astron. Soc.* **2018**, *475*, 2326−2343.
(40) Luo, H. X.; Jia, P. F.; Qiao, S. Q.; Duan, S. K. Enhancing Electronic Nose Performance Based on a Novel QPSO-RBM Technique. Sens. *Sens. Actuators, B* **2018**, *259*, 241−249.
(41) Stephens, C. R.; Huerta, H.; Linares, A. When is the Naive Bayes Approximation Not So Naive? *Machine Learning* **2018**, *107*, 397−441.
(42) Jiang, W. Q.; Shen, Y. F.; Ding, Y. F.; Ye, C. Y.; Zheng, Y.; Zhao, P.; Liu, L. L.; Tong, Z.; Zhou, L. F.; Sun, S.; Zhang, X. C.; Teng, L. S.; Timko, M. P.; Fan, L. J.; Fang, W. J. A Naive Bayes Algorithm for Tissue Origin Diagnosis (TOD-Bayes) of Synchronous Multifocal Tumors in the Hepatobiliary and Pancreatic System. *Int. J. Cancer* **2018**, *142*, 357−368.
(43) Tian, J.; Morillo, C.; Azarian, M. H.; Pecht, M. Motor Bearing Fault Detection Using Spectral Kurtosis-based Feature Extraction Coupled with K-nearest Neighbor Distance Analysis. *IEEE Trans. Ind. Electron.* **2016**, *63*, 1793−1803.
(44) Richter, C.; King, E.; Falvey, E.; Franklyn-Miller, A. Supervised Learning Techniques and Their Ability to Classify a Change of Direction Task Strategy Using Kinematic and Kinetic Features. *J. Biomech.* **2018**, *66*, 1−9.
(45) Mohammed, A. A.; Minhas, R.; Wu, Q. M. J.; Sid-Ahmed, M. A. Human Face Recognition Based on Multidimensional PCA and Extreme Learning Machine. *Pattern Recognition* **2011**, *44*, 2588−2597.
(46) Guru, D. S.; Suhil, M.; Raju, L. N.; Kumar, N. V. An Alternative Framework for Univariate Filter Based Feature Selection for Text Categorization. *Pattern Recog. Lett.* **2018**, *103*, 23−31.
(47) Staton, M.; Ciciurkaite, G.; Havens, J.; Tillson, M.; Leukefeld, C.; Webster, M.; Oser, C.; Peteet, B. Correlates of Injection Drug Use Among Rural Appalachian Women. *J. Rural Health* **2018**, *34*, 31−41.
(48) Shang, L.; Guo, W. C.; Nelson, S. O. Apple Variety Identification Based on Dielectric Spectra and Chemometric Methods. *Food Anal. Method* **2015**, *8*, 1042−1052.

DOI: 10.1021/acssensors.8b00329
ACS Sens. 2018, 3, 1531−1538